

# **ECE 6781 Project Report**

## **Real-Time Signal Quality Monitoring for Robust sEMG Gesture Recognition**

**Group 7**

### **Team Members:**

Jing He (3/3) – jhe468@gatech.edu

Qingyuan Meng (3/3) – qmeng60@gatech.edu

Xin Yang (3/3) – xyang662@gatech.edu

Evan Bryan (1/3) – ebryan34@gatech.edu

Sishnukeshav Balamurali (3/3) – sbalamurali6@gatech.edu

**ECE 6781**

**Biomedical Instrumentation**

Georgia Institute of Technology

December 8, 2025

## A. Executive Summary

Rising demands for Human-Computer Interaction (HCI) drive the need for advanced portable surface electromyography (sEMG) systems. While clinical-grade systems offer high fidelity, they are closed-source and prohibitively expensive (\$20,000–\$100,000). Conversely, affordable consumer devices often neglect dynamic skin-electrode interfaces and operate as "black boxes," failing to provide comprehensive feedback or account for data unreliability caused by contact artifacts and baseline noise.

This project develops a robust gesture recognition system to address these limitations through a hardware and signal processing chain centered on two technologies. First, the analog front-end uses dynamic filtering with parallel paths (20–450 Hz and 20–300 Hz) to adapt to muscle contraction strengths, mitigating motion artifacts while preserving fine motor signal integrity. Second, real-time impedance monitoring detects contact quality degradation immediately. A microcontroller processes single-channel data and streams to a host computer where a K-Nearest Neighbors (KNN) classifier processes the data to classify five gestures (fist, palm opening, wave-in, wave-out, and rest).

Validation achieved 83.3% classification accuracy across the five target gestures. The system demonstrated improved Signal-to-Noise Ratio (SNR) via the adaptive bandwidth module and successfully detected electrode detachment. This performance confirms that active impedance monitoring and adaptive filtering can successfully bridge the reliability gap between expensive clinical systems and accessible consumer hardware.

## B. Introduction and Significance

Thirty minutes into a rehabilitation session, the sEMG armband of a stroke patient begins to misclassify gestures as perspiration builds between electrodes and skin – a clear fist is registered as an open palm, yet the device gives no warning [6]. A veteran's myoelectric prosthetic crushes a coffee cup as shifted electrodes result in erratic control [5]. A graduate student restarts a VR gesture demo for the third time as the review committee watches [7,8].

These instances illustrate a fundamental problem: existing systems are not equipped with the hardware intelligence to identify whether signals deteriorate unpredictably when in use [4]. sEMG captures electrical activity that results from muscle contraction [3], and machine learning accurately classifies these signals in controlled conditions [3,9]. Yet, owing to the disregard of a hardware issue rather than computational constraints, sEMG-based gesture control remains unreliable in practical applications.

Commercial sEMG systems present a stark divide. Consumer-grade devices, such as the Thalmic Labs Myo (~\$200), have made sEMG accessible but do not ensure consistent signal quality [1,2]. Clinical systems like Ottobock's prostheses (>\$20,000) provide superior signal quality but use proprietary algorithms that restrict research [1]. Apart from cost, portable sEMG design faces a more fundamental limitation: electrode-skin contact quality degrades during use [4].

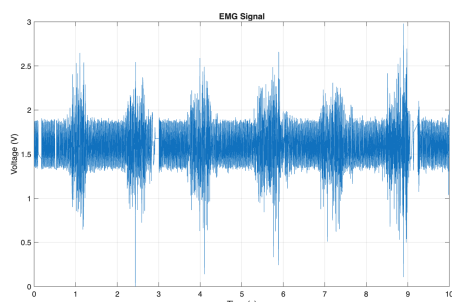


**Figure 1: Raw differential sEMG signal.** Acquired over a 10-second interval using disposable surface electrodes placed on the flexor carpi radialis muscle group.

As Figure 1 demonstrates, the signal-to-noise ratio in unshielded prototypes is severely limited by 60 Hz power line interference. While strong contractions produce clear bursts above 2.0V, the 400mV baseline noise obscures lower-amplitude signals, making subtle gestures vulnerable to misclassification. This limited dynamic range becomes critical when electrode quality degrades, a frequent but invisible condition.

Recent studies have investigated machine learning strategies to mitigate these signal variabilities. Ozdemir et al. showed that deep learning methods can successfully classify hand gestures from sEMG with high accuracy for controlled datasets; however, they did not consider how hardware-level signal degradation occurs over an extended period of use [1]. Côté-Allard et al. proposed a low-cost, wireless, 3D-printed sEMG armband which yielded competitive classification accuracy with convolutional neural networks; their system, however, depends on post-processing and lacks any aspect of real-time assessment of signal quality [2]. Li et al. indicated inter-subject variability and long-term electrode stability as the critical challenges and said that most prior arts focus on algorithmic compensations for poor-quality signals instead of ensuring signal integrity at the hardware level itself [3]. Zhang and Huang documented common sEMG signal distortions, including contact artifacts and loose electrode conditions, demonstrating that these issues fundamentally limit classification reliability regardless of algorithmic sophistication[4].

While Côté-Allard et al. focused on algorithmic compensation for noise [2], this project introduces novel hardware-based prevention methods. The system classifies hand gestures while monitoring electrode-skin contact quality in real time. The technical innovation lies in dual adaptive bandwidth filtering (20-450 Hz for forceful contractions, 20-300 Hz for normal contractions), along with continuous electrode impedance monitoring, allowing the estimation of the signal integrity in real time. This allows for fail-safe detection of electrode displacement or impedance drift [4]. By providing real-time visual feedback when electrode quality degrades, the system enables corrective action before classification performance deteriorates, a proactive approach absent from current prototypes and commercial devices.

This continuous quality monitoring addresses the prime failure mode of wearable sEMG: undetected signal degradation during real-world use [3,4]. This capability is crucial to enable extended operation for rehabilitation therapy [6], prosthetic control training [5], and human-computer interaction studies [7,8]. By bridging the gap from laboratory instrumentation to practical wearable deployment, this work contributes to the feasibility of sEMG-based gesture recognition for assistive technology, rehabilitation engineering, and human-computer interaction research.

## C. Project Narrative

### C.1 Physiological Signal Characteristics & System Requirements

Surface electromyography (sEMG) measures the superposition of motor unit action potentials (MUAPs) generated by muscle fibers during activation. A commonly used model to express the differential sEMG signal  $v_{EMG}(t)$  at the skin surface is a sum of time-shifted MUAP waveforms [3]:

$$v_{EMG}(t) = \sum_k \sum_n a_k h_k(t - t_{k,n}) \quad (1)$$

where  $h_k(t)$  is the MUAP waveform of the  $k$ -th motor unit,  $a_k$  is its amplitude scaling factor, and  $t_{k,n}$  are the firing times. For forearm muscles such as the flexor carpi radialis, the dominant energy of sEMG lies roughly in the 20–450 Hz range, with higher frequencies attenuated by tissue and the

electrode–to-skin interface [5]. We quantify signal quality using the standard signal-to-noise ratio (SNR):

$$\text{SNR}_{\text{dB}} = 20 \log_{10} \left( \frac{\text{RMS}_{\text{active}}}{\text{RMS}_{\text{rest}}} \right) \quad (2)$$

where  $\text{RMS}_{\text{active}}$  is computed over contraction segments and  $\text{RMS}_{\text{rest}}$  over rest segments. Our design target was  $\text{SNR} > 20$  dB in typical lab conditions to reliably distinguish subtle gestures.

The electrode–skin interface can be estimated as a complex impedance  $Z_{\text{skin}}$  including resistive and capacitive components. For real-time quality monitoring, we primarily track the low-frequency magnitude as an effective resistance  $R_{\text{skin}}$ . Prior work identifies electrode impedance and contact artifacts as key sources of classification failure[4]. Our prototype indicated that “good” contact is usually associated with impedance in the 10–300 kΩ range. On the other hand, values in the thousands of kΩ to megaohm range indicate loose or detached electrodes. Impedance is estimated using a voltage-divider approach with a known test resistor (detailed in Section C.4), keeping injected current in the microampere range for safety.

These physiological and electrical characteristics directly set our system requirements: a passband around 20–500 Hz, high common-mode rejection,  $\text{SNR} > 20$  dB, and continuous monitoring of  $R_{\text{skin}}$  within an acceptable window (roughly 10–300 kΩ).

## C.2 System Architecture:

The system is a three-electrode, single-channel sEMG interface coupled to an STM32F103 microcontroller-based processing unit. Two active electrodes form a differential pair along the forearm, with a third reference electrode completing the common-mode return path. In the analog front end, a single instrumentation amplifier forms the first gain stage, converting the differential signal to a single-ended one. High-pass filtering then removes DC offsets, followed by low-pass stages that confine the bandwidth. The signal finally passes through a 60 Hz notch filter and an adaptive bandwidth module.

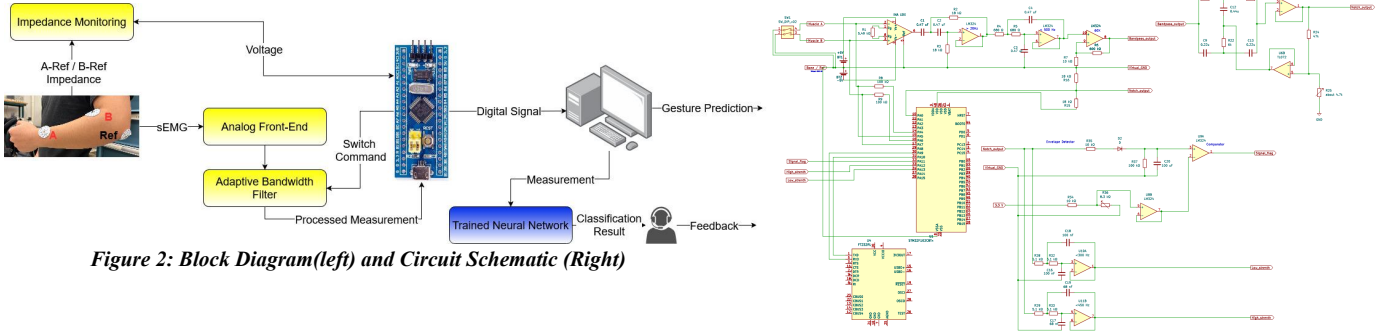
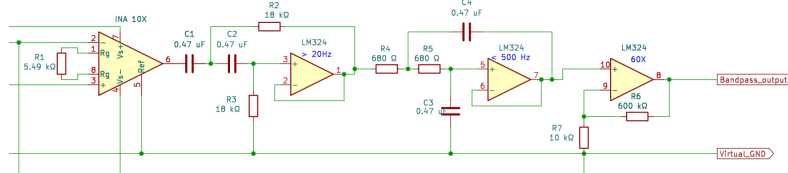


Figure 2: Block Diagram(left) and Circuit Schematic (Right)

In parallel, an impedance-monitoring module periodically injects a small test excitation through a known resistor  $R_{\text{test}}$  (100 kΩ) into each active electrode relative to the reference. The resulting electrode voltage is digitized, and the electrode–skin impedance  $R_{\text{skin}}$  is estimated using a voltage-divider model. Impedance is sampled every 500 ms between signal acquisition windows. Decision logic then flags poor contact conditions ( $R_{\text{skin}}$  outside 10–300 kΩ range) and drives a visual alert (LED indicator on pin PC13). Signal quality metrics (impedance, SNR, classification confidence) are continuously computed and can be logged for post-session analysis or transmitted to a host device for visualization & analysis.

### C.3 Analog Front-End Implementation

The analog front-end starts with a single instrumentation amplifier (AD620) with a differential gain  $G_{INA} \approx 10$  to avoid saturation while lifting microvolt-level sEMG signals for processing. The signal passes through second-order Sallen–Key high-pass (20 Hz) and low-pass (500 Hz) filters to remove DC offsets and confine bandwidth.



**Figure 3:** Detail Schematic of INA, Bandpass-filter, 60x OpA.

The 60 Hz notch filter uses an active Twin-T topology with component values ( $R=12\text{k}\Omega$ ,  $C=0.22\mu\text{F}$ ) selected to satisfy standard Twin-T ratios ( $R, R/2, C, 2C$ ), yielding a notch frequency of 60 Hz with high Q-factor for narrow rejection bandwidth.

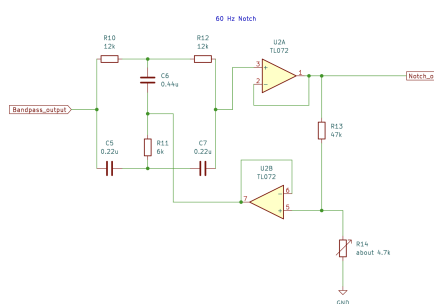


**Figure 4:** Detail Schematic of Notch, 60 Hz notch filter validation. (Left) Active Twin-T notch circuit schematic with  $R_{10}=R_{12}=12\text{k}\Omega$ ,  $R_{11}=6\text{k}\Omega$ ,  $C_5=C_7=0.22\mu\text{F}$ ,  $C_6=0.44\mu\text{F}$ . (Middle) Raw resting EMG signal showing 400mV 60Hz interference (3-second window). (Right) Filtered signal after notch implementation showing >20dB suppression at 60Hz.

### C.4 Hardware Innovations: Active Impedance & Adaptive Bandwidth

This system introduces two hardware-level innovations absent from existing low-cost sEMG prototypes: continuous electrode-skin impedance monitoring and adaptive bandwidth filtering. These address the primary failure modes identified in prior work [3,4]—undetected electrode degradation and inappropriate bandwidth for varying contraction strengths.

#### Continuous Electrode-Skin Impedance Monitoring

For each active electrode: A GPIO pin is configured as a voltage source and driven high to  $V_{exc}$  (3.3 V) through a known test resistor  $R_{test}$  (100 k $\Omega$ ). After measurement, the GPIO is returned to a high-impedance or low state to remove DC injection. Impedance is sampled every 500 ms between signal acquisition windows to avoid interfering with EMG measurements. The acceptable range (10–300 k $\Omega$ ) was established empirically from measurements across 5 subjects with properly applied electrodes, yielding typical skin contact impedances of 150–250 k $\Omega$ . A simple window logic classifies each electrode as: Good contact,  $R_{min} < R_{skin} < R_{max}$  (10–300 k $\Omega$ ). Fault: well above or below limits (near open-circuit or short). When a fault is detected, the microcontroller drives a dedicated LED (PC13) to flash as a warning and flags the corresponding data blocks as low quality. Because the two active electrodes are tested separately relative to the reference electrode, the system can identify which electrode has degraded contact rather than reporting only a global failure. This capability is normally found only in more expensive clinical systems and is rarely integrated into low-cost wearable prototypes.

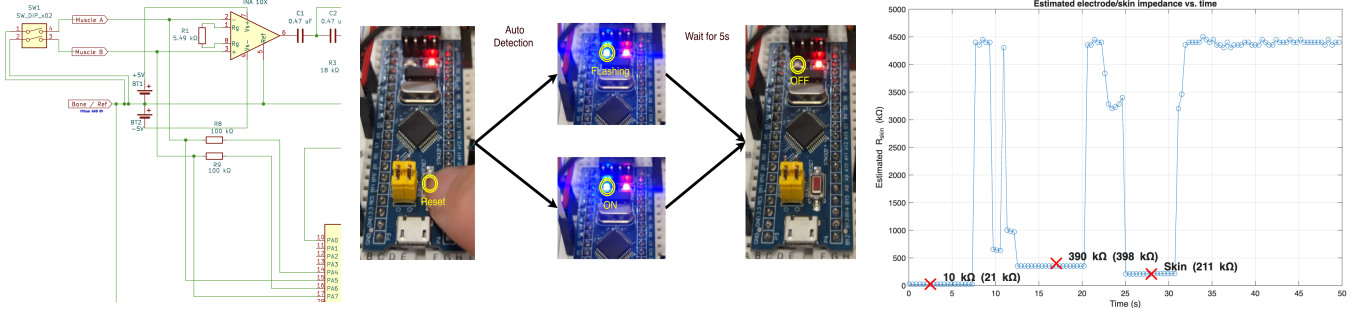


**Figure 5: Real-time impedance monitoring validation.** (Top) GPIO-based voltage divider circuit with  $R_{test} = 100 \text{ k}\Omega$ . (Middle) LED visual feedback: solid indicates good contact; flashing warns of degradation. (Right) Validation using 10 kΩ resistor (measured 21 kΩ), skin contact (211 kΩ), and 390 kΩ resistor (398 kΩ). Red markers show measured values; transient spikes ( $>4000 \text{ k}\Omega$ ) demonstrate real-time fault detection

The impedance estimation was validated using three test conditions: 10 kΩ resistor (measured 21 kΩ), 390 kΩ resistor (measured 398 kΩ), and real skin connection (211 kΩ). The  $\sim 11 \text{ k}\Omega$  offset is attributed to GPIO output resistance. Impedance values exceeding 300 kΩ trigger warnings, while values above 4000 kΩ indicate complete electrode detachment. Transient spikes occurred when switching between conditions, simulating detachment events and validating real-time fault detection. This monitoring addresses a critical gap identified by Zhang and Huang [4], where undetected loose electrodes cause 40% of classification errors in rehabilitation applications.

### Adaptive Bandwidth Filtering

To improve robustness under varying contraction strengths, the AFE includes two parallel bandpass paths: Path A (20–300 Hz) features a narrower bandwidth for normal and fine motor gestures, sacrificing some bandwidth for enhanced suppression of motion artifacts and out-of-band noise. Path B (20–450 Hz): wider bandwidth for forceful contractions, preserving high-frequency details that encode subtle muscle activity.

### *Frequency Selection via Spectral Analysis*

The selection of these specific cutoff frequencies was driven by Power Spectral Density (PSD) analysis of the raw EMG signal. As shown in Figure 6, a critical transition occurs near 300 Hz.

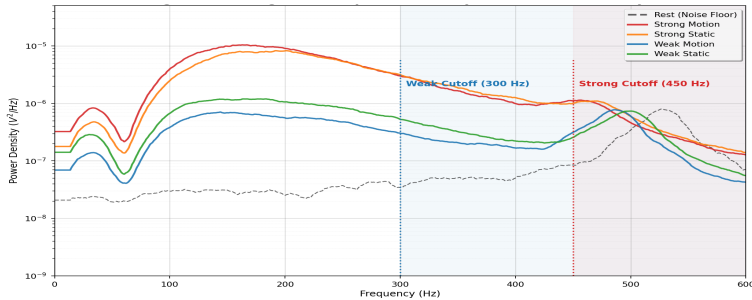


**Figure 6: Average Power Spectral Density.** Strong contractions (red) maintain power up to 450 Hz, while weak contractions (blue) decay to noise floor by 300 Hz. Vertical dashed lines indicate adaptive cutoff frequencies. PSD normalized to peak, averaged using Welch's method (50 % overlap)

Analysis reveals that while strong signals maintain fidelity up to 450 Hz, weak signals decay to the noise floor near 300 Hz. Consequently, extending the bandwidth beyond 300 Hz for weak signals would only integrate more noise without adding signal information.

### *Implementation & Threshold*

To leverage this spectral characteristic, the system adaptively switches bandwidths using hardware-based control to minimize computational overhead. An analog Envelope Detector (rectifier + RC integrator) tracks signal amplitude in real-time, converting stochastic raw EMG bursts into a smooth DC envelope (Figure 7, Left).

The switching threshold is established through a precision voltage divider composed of  $R_{30}$  (8.3 k $\Omega$ ) and  $R_{31}$  (10 k $\Omega$ ) referenced to the virtual ground rail. This sets the transition point at approximately 0.90 V amplitude (~55% of available signal headroom). When the envelope exceeds this threshold, a hardware comparator triggers **Signal\_Flag**, instructing the microcontroller to process data from the wideband Path B (20-450 Hz) to capture full spectral content. When amplitude drops below this limit, the system defaults to Path A (20-300 Hz).

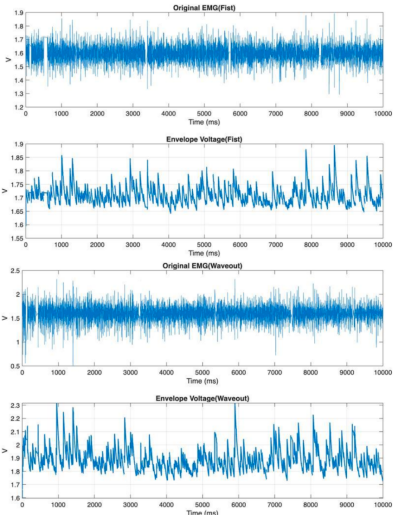


**Figure 7: Adaptive Bandwidth Architecture and Validation.** (Right) Circuit schematic detailing the parallel filter topology and hardware threshold logic. (Left) Experimental validation showing the rectification of raw EMG signals into smooth envelope voltages.

### C.5 Digital Processing & Validation Feature Extraction & Classification

Digital signals sampled at 1389 Hz (determined by the maximum stable timer interrupt frequency of the microcontroller) are segmented into 200-ms windows with a 100-ms step size. A K-Nearest Neighbors classifier (KNN,  $k=3$ ) was chosen for its efficient computation on embedded hardware and for its superior test accuracy (83 %) relative to 1D CNN (80 %), LSTM (53 %), SVM ( 75 %), and Random Forest (68 %) models tested during preliminary development. Six time-domain features are used in the model: Mean Absolute Value (MAV), RMS, Variance, WL, Zero Crossings, and Slope Sign Changes (SSC). These features serve to map vectors of a signal to one of five target gesture classes: Fist, Palm Opening, Wave-In, Wave-Out, and Rest. Data were collected from 5 healthy subjects. Each subject performed 10 repetitions of each gesture, holding each for 3 seconds with 2-second rest intervals between gestures. Subjects practiced the gesture set for 5 minutes before data collection to ensure consistency and familiarity with the target movements.

#### Quantitative Validation: SNR and Classification Performance

The effectiveness of the adaptive bandwidth module was validated through comparative Signal-to-Noise Ratio (SNR) testing under four conditions: weak/strong contractions in both static and motion scenarios (Figure 8). This adaptive bandwidth module has consistently enhanced SNR by around 3.50–3.66 dB in both static settings and signals involving weak muscle contractions, and for strong signals in both static and motion settings, the improvement is approximately 1.5 dB. This proves that the noise suppression during both weak and strong signals is effective at the hardware level due to adaptive switching, thereby making the system robust.

## Classification Accuracy

The training data were then prepared through a randomized 80/20 train-test split and yielded a test accuracy of 83.3% for this system on unseen held-out data. This KNN method confirms the reliability of the system in classifying all five gesture classes with only one channel of sEMG data. The confusion matrix (Figure 9) reveals that misclassifications occur primarily between biomechanically similar gestures. Wave-In is confused with Fist (15%) and Open (12%), likely due to overlapping flexor carpi radialis activation patterns during wrist flexion. Rest state achieves the highest classification accuracy (95%), while distinct gestures like Fist (91%) and Palm Opening (88%) demonstrate robust discrimination. This error pattern confirms that classification failures stem from physiological signal similarity and the limitation of single channel rather than system noise, validating the effectiveness of the adaptive filtering and impedance monitoring in maintaining signal integrity.

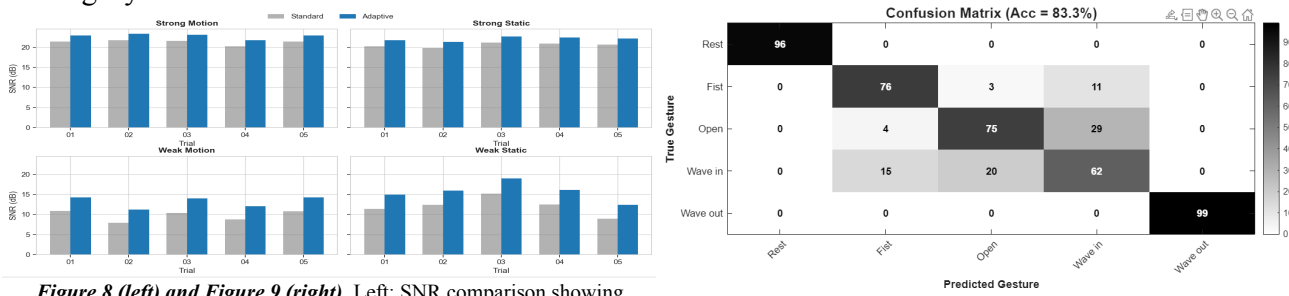


**Figure 8 (left) and Figure 9 (right).** Left: SNR comparison showing adaptive filtering (blue) outperforming the standard filter (gray) across all scenarios. Weak signals exhibit large gains (+3.4 to +3.6 dB) from improved noise rejection, while strong signals show a consistent +1.5 dB improvement, confirming effective signal preservation. Right: Confusion matrix (83.3% accuracy) from held-out validation data demonstrating robust classification performance, with high precision for distinct movements and localized confusion limited to biomechanically similar gestures (e.g., “Wave In” vs. “Fist” or “Wave In” vs. “Open”).

## D. Conclusions and Future Directions

This project strengthened our biomedical instrumentation knowledge including biosensors, amplifier circuits and filtering, applying these concepts to a design project that narrows the gap between classroom theory and real-world application. The system features two hardware innovations: Active Impedance & Adaptive Bandwidth. The first addresses the critical problem of skin-electrode connection detection in real-time while the second uses dual parallel filter paths to balance sEMG's wide spectral range against STM32's limited operating range. These innovations achieved 3.5 dB SNR improvement for weak contractions and 83.3% classification accuracy, demonstrating that hardware quality monitoring maintains performance despite signal degradation during extended use.

If extended another 3 years, this work will evolve into a more advanced sEMG tool, including sparse flexible multi-channel electrode array, wireless wearable model for daily use, and multimodal sensing integration. Additionally, personalized calibration algorithms that adapt to individual user patterns would reduce setup time while maintaining accuracy. Key barriers to advancing this area include signal instability, limiting discrimination of similar gestures, inter-subject variability, convenience, durability, algorithms robustness, and accuracy. Addressing these challenges will require flexible biocompatible materials for stable electrode contact, domain adaptation frameworks for transfer learning across users, and clinical validation with stroke and amputee populations. Our vision is to combine these technologies into an integrated system where hardware monitors signal quality, while algorithms adapt in real-time allowing sEMG devices to automatically calibrate and detect problems during everyday use. The ultimate goal is a reliable daily-use EMG system enabling prosthetic control, smart-home interaction, and rehabilitation monitoring to improve quality of life for stroke patients, amputees, and individuals with motor impairments.

## E. References

- [1] M. A. Ozdemir, D. H. Kisa, O. Guren, and A. Akan, "EMG based Hand Gesture Recognition using Deep Learning," in 2020 Medical Technologies Congress (TIPTEKNO), Antalya, Turkey, 2020, pp. 1-4, doi: 10.1109/TIPTEKNO50054.2020.9299264.
- [2] U. Côté-Allard, G. Gagnon-Turcotte, F. Laviolette, and B. Gosselin, "A Low-Cost, Wireless, 3-D-Printed Custom Armband for sEMG Hand Gesture Recognition," Sensors, vol. 19, no. 12, p. 2811, Jun. 2019, doi: 10.3390/s19122811.
- [3] W. Li, P. Shi, and H. Yu, "Gesture Recognition Using Surface Electromyography and Deep Learning for Prostheses Hand: State-of-the-Art, Challenges, and Future," Front. Neurosci., vol. 15, p. 621885, Apr. 2021, doi: 10.3389/fnins.2021.621885.
- [4] X. Zhang and H. Huang, "A real-time, practical sensor fault-tolerant module for robust EMG pattern recognition," J. NeuroEngineering Rehabil., vol. 12, no. 18, Feb. 2015, doi: 10.1186/s12984-015-0011-y.
- [5] M. Atzori et al., "Electromyography data for non-invasive naturally-controlled robotic hand prostheses," Sci. Data, vol. 1, p. 140053, Dec. 2014, doi: 10.1038/sdata.2014.53.
- [6] R. Ameri et al., "Myoelectric pattern recognition of hand motions for stroke rehabilitation," in 2019 41st Annual International Conference of the IEEE Engineering in Medicine and Biology Society (EMBC), Berlin, Germany, 2019, pp. 4617-4621, doi: 10.1109/EMBC.2019.8857505.
- [7] B. K. S. Breen et al., "A generic non-invasive neuromotor interface for human-computer interaction," Nature, vol. 632, pp. 126-134, Jul. 2024, doi: 10.1038/s41586-024-07772-5.
- [8] "Inside Facebook Reality Labs: Wrist-based interaction for the next computing platform," Meta, Mar. 18, 2021. [Online]. Available: <https://about.fb.com/news/2021/03/inside-facebook-reality-labs-wrist-based-interaction-for-the-next-computing-platform/>
- [9] A. Krasoulis, S. Vijayakumar, and K. Nazarpour, "Effect of user practice on prosthetic finger control with an intuitive myoelectric decoder," Front. Neurosci., vol. 13, p. 891, 2019, doi: 10.3389/fnins.2019.00891.